Dalton Transactions

COMMUNICATION

View Article Online
View Journal | View Issue

Cite this: *Dalton Trans.*, 2016, **45**, 3251

Received 14th October 2015,
Accepted 20th January 2016

DOI: 10.1039/c5dt04027b

www.rsc.org/dalton

Alkynyl bridged cyclometalated Ir_2M_2 clusters: impact of the heterometal in the photo- and electro-luminescence properties†

Julio Fernández-Cestau,‡[a] Nora Giménez,[a] Elena Lalinde,*[a] Patricia Montaño,[a] M. Teresa Moreno,[a] Sergio Sánchez,[b] Michael D. Weber[c] and Rubén D. Costa*[c]

We report two unprecedent alkynyl bridging cyclometalated clusters $[Ir_2M_2(ppy)_4(\mu\text{-}C{\equiv}CC_6H_4\text{-}OMe_3)_4]$ where M is Ag (2) and Cu (3), which display distinctive luminescence properties. While 2 features a green phosphorescence/electroluminescence nature located at the ppy ligands (^{3}LC), 3 shows an orange emission confined to the metals and alkynyl groups having a mixed ^{3}L′C/^{3}L′ MCT/^{3}MMCT (L′ = alkynyl) nature.

Phosphorescent cyclometalated Ir^{III} complexes have aroused enormous interest due to their outstanding photo- and electroluminescence properties, which are well suited for optoelectronic applications, such as organic light-emitting diodes (OLEDs), light-emitting electrochemical cells (LECs), sensors or biological cell imaging.[1] In particular, homoleptic and heteroleptic mononuclear Ir^{III} complexes have been extensively investigated by means of both experimental and theoretical studies to master both the color and efficiency of the emission, providing a clear understanding of the relationship between the structure and photophysical properties.[1a–d,2] Although much less explored, $Ir(C\hat{}N)_2$ motifs have also been used as building blocks in linear or branched multinuclear 1D systems to study photoinduced energy and electron transfer processes and to form interesting homo and hetero multimetallic luminescent arrays.[3]

Besides the latter, owing to their rich σ- and π-bonding versatility along with the metallophilic interactions, the alkynyl ligands are known to be particularly successful to form very stable d^8 and d^{10} homo and heterometallic complexes with fascinating structures and interesting photophysical properties, including solid-state mechanochromic, thermochromic, and sensing behaviour.[4] However, their application in optoelectronic devices has been barely explored.[4a,d] Thus, it is worthwhile to investigate the photophysical properties arising from the combination of $Ir(C\hat{}N)_2$ units and coinage alkynyl motifs in the same molecule, which has not been explored yet. In these systems, the emission properties could be attributed to the Ir^{III} chromophore, the heterometal–alkynyl unit or to exhibit a unique nature derived from specific short-range interactions favoured by the alkynyl bridging ligands. In this communication, we wish to report the synthesis, the molecular and electronic structures, as well as photo- and electro-luminescence properties of two tetranuclear luminescent complexes $[Ir_2M_2(ppy)_4(\mu\text{-}C{\equiv}CC_6H_4OMe\text{-}3)_4]$ where M is Ag (**2**) or Cu (**3**), together with the diiridium precursor $[Ir_2(ppy)_4(\mu\text{-}C{\equiv}CC_6H_4OMe\text{-}3)_2]$ (**1**). Despite their similar structures, **2** and **3** display distinct optical properties, which have been interpreted with the aid of theoretical calculations based on the density-functional theory (DFT and its time-dependent approach TD-DFT).

Recently, a series of dinuclear alkynyl Ir^{III} complexes $[Ir_2(ppy)_4(\mu\text{-}C{\equiv}CR)_2]$ where R = Tol, C_6H_4OMe-4, 1-Np, Bu^t, $SiMe_3$ have been synthesized in our laboratory *via* the reaction of $[Ir_2(ppy)_4(\mu\text{-}Cl)_2]$ with the corresponding alkynyl lithium reagent.[5] During the investigation of possible routes to prepare this type of complexes, we discovered that the dinuclear chloride bridging precursor $[Ir_2(ppy)_4(\mu\text{-}Cl)_2]$ reacts with the polymeric silver derivative $[Ag(C{\equiv}CC_6H_4OMe\text{-}3)]_n$ to yield the tetranuclear complex **2** as a yellow microcrystalline solid in high yield (75%). Similar to this traditional reaction, the latter and the related Cu^I copper derivative **3** are straightforwardly generated *via* a quasi-quantitative reaction of the dinuclear alkynyl bridged complex $[Ir_2(ppy)_4(\mu\text{-}C{\equiv}CC_6H_4OMe\text{-}3)_2]$ **1**, which is prepared for first time for this work, with the polymeric derivatives $[M(C{\equiv}CC_6H_4OMe\text{-}3)]_n$ (M = Ag, Cu) with a yield of M = Ag 93%; Cu 91% (Scheme 1). The formation of luminescent alkynyl based heterometal clusters by using poly-

[a]*Departamento de Química – Centro de Investigación en Síntesis Química. Universidad de La Rioja, 26006 Logroño, Spain. E-mail: elena.lalinde@unirioja.es*
[b]*School of Chemistry, University of Manchester, Oxford Road, Manchester M13 9PL, UK*
[c]*Department of Physical and Chemistry I, Excellence Cluster of Engineering of Advanced Materials (EAM), Friedrich-Alexander-Universität Erlangen-Nürnberg, Egerlandstrasse 3, 91058 Erlangen, Germany. E-mail: ruben.costa@fau.de*

†Electronic supplementary information (ESI) available: Synthetic procedures, full set of characterization data, crystallographic, photophysical and theoretical data. CCDC 1429228, 1429229 and 1444008. For ESI and crystallographic data in CIF or other electronic format see DOI: 10.1039/c5dt04027b

‡Present address: Wolfson Materials and Catalysis Centre, School of Chemistry, University of East Anglia, Norwich, NR4 7TJ. Fax: +44 016035 92044.

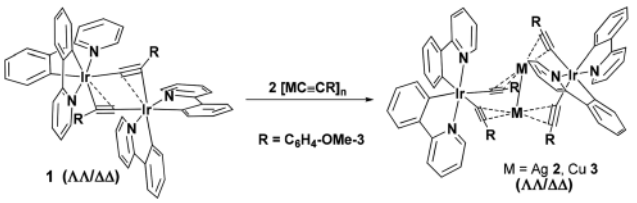

Scheme 1 Synthesis of $[Ir_2M_2(ppy)_4(\mu\text{-}C{\equiv}CC_6H_4OMe\text{-}3)_4]$ (M = Ag **2** or Cu **3**).

meric coinage $[M(C{\equiv}CR)]_n$ derivatives as precursors has been reported,[4c,f,6] but their employment to assemble Ir^{III} phosphorescent cyclometalated fragments $Ir(C^{\wedge}N)_2$ is unprecedented. Unfortunately, the attempts to obtain the analogous Ir_2Au_2 cluster both by reaction of **1** with $[Au(C{\equiv}CC_6H_4OMe\text{-}3)]_n$ or by a transmetalation reaction between the Ir_2Ag_2 cluster **2** and $[AuCl(SMe_2)]$ were unsuccessful.

All **1–3** complexes were characterized by analytical and spectroscopic techniques – see the ESI† for more details, Fig. S1–S15† – and their molecular structures were confirmed by X-ray crystallography. The dinuclear complex **1** is generated only as the racemate (ΛΛ/ΔΔ) and the clusters **2** and **3** feature the retention of the configuration at the Ir^{III} centres (ΛΛ/ΔΔ form) – Fig. 1, S16–S20, Tables S1–S4.†

In both clusters, the two enantiomers are present in the unit cell that shows a space group triclinic $P\bar{1}$ for **2** and tetragonal $I\bar{4}$ for **3**. The forms shown in Fig. 1 are ΛΛ and ΔΔ for **2** and **3**, respectively. Both clusters are similarly constructed by two unprecedent anionic building blocks, bis(alkynyl)bis(phenylpyridinyl)iridate(III), $\{Ir(ppy)_2(C{\equiv}CR)_2\}^-$, and two Ag^I (**2**) or Cu^I (**3**) ions held together by π···C≡CM^I bonds and $M^I\cdots M^I$ interactions. The two bidentate bridging iridadiyne fragments $[Ir](C{\equiv}C)_2$ are oriented almost perpendicular to each other, the dihedral angles being 84.2° for **2** and 79.30° for **3** (Fig S17†). The metal centres form a rhomboidal skeleton with a *trans* annular $M^I\cdots M^I$ separation [2.9985(7) **2**; 2.732(2) Å **3**], shorter than the sum of van der Waals radii (3.34 and 2.8 Å for Ag^I and Cu^I) and in the range typical for metallophilic interactions.[7] With regard to the Ir–M^I distances, the shortest distances [3.4654(7) Å in **2** and 3.154(1) Å in **3**] are longer than those noted in other heterometallic Ir–M^I clusters[7c] (*i.e.*, $[Ir_2M_4(C{\equiv}CR)_8(PPh_3)_2]$ mean 3.08 for Ag and 2.88 Å for Cu),[6a] excluding any significant $d^6\cdots d^{10}$ bonding interactions. The Ir^{III} centres are coordinated to two cyclometalated ppy ligands and two σ-alkynyl carbons, adopting typical *C,C-cis* and *N,N-trans* configurations, whereas the Ag^I (**2**) or Cu^I (**3**) ions are dicoordinately bonded to two staggered ethynide units mutually *trans* of each Ir^{III} block. The Cu–C_α,C_β distances [1.991(10)–2.102(10) Å] in **3** are shorter than those noted in Ag–C_α,C_β [2.287(6)–2.305(6) Å] in **2**, a feature that is in accordance with the lower ν(C≡C) stretching vibration found in **3** (1952 cm^{-1}) in relation to **2** (1990, 1964 cm^{-1}). This indicates, in line with previous observations,[4c,f] that the η^2-alkyne interaction is stronger in the Cu^I than in the Ag^I complex. In **3**, one C_6H_4OMe-3 ring is disordered over two positions (occupancy 0.75/0.25), although it does not affect the essential parameters of the structure. The structural data given refer to the majority component of the disorder. For **2**, the crystal structure reveals the formation of a zigzag chain stabilized by weak O(OMe)···H(ppy) interactions and offset face-to-face π–π stacking between ppy moieties (Fig. S18†), whereas in **3** each cluster is involved in two bad directed π···π contacts reinforced with CH(ppy)···(C≡C) interactions, which leads to a more compact network (Fig. S20†).

The electrochemical properties were examined by cyclic voltammetry (Fig. S21†) and the data are shown in Table S5.† **1** displays in THF a single irreversible 2 e^- oxidation at 0.65 V, whereas in CH_2Cl_2 it shows two oxidation waves (i_{pa}/i_{pc} < 1) with peak potentials (E_{pa}) at 0.57 and 0.81 V, formally ascribed to two sequential Ir^{III}/Ir^{IV} processes. The separation of the Ir^{III}/Ir^{IV} waves (ΔE_{pa} 240 mV) suggests electronic communication between the iridium centres, as in previously related doubly bridged arylacetylide diiridium complexes.[5] The tetranuclear clusters display in THF one (0.94 V for **2**) or two (0.82 and 0.98 V for **3**) irreversible oxidations, which are anodically shifted compared to **1**, indicating that the highest-occupied molecular orbitals (HOMOs) are substantially stabilized in relation to that of **1**. At a first glance, this result could be ascribed to the lower π-donor ability of the alkynyl ligand upon an η^2-bonding interaction with the acidic Ag^I and Cu^I ions, rendering the Ir^{III} metal centre oxidation more difficult in the clusters. Since the η^2-alkyne–M bonding interactions are stronger for Cu^I in relation to Ag^I, **3** should exhibit a higher oxidation potential than **2**, however, this is opposite to what we noted. The irreversible nature of the oxidation processes suggests a relatively high contribution of the ligands in the HOMOs, as confirmed by calculations. Here, DFT calculations and atomic orbital composition analyses on the optimized S_0 geometries revealed that their frontier orbitals are quite different (Tables S7–S9, Fig. S28 and S29†). In detail, the HOMO of **2** is localized in one of the Ir^{III} fragments (Ir^{III} 40%; ppy 40%; C≡CR 17%), with a small contribution of one Ag^I(5sp) (2%). However, **3** shows a delocalized HOMO between both the Ir^{III} fragments with a higher contribution of the alkynyl groups (36%) and a lower contribution of ppy units (22%) and Ir^{III} (34%) than **2**. The 0.1 eV energy difference

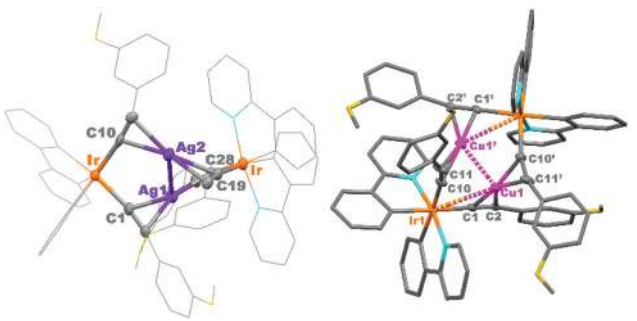

Fig. 1 Crystal structures of **2**·2CH_2Cl_2 (left) and **3** (right). Hydrogen atoms are omitted for clarity. M···M distances (Å): Ag1···Ag2 2.9985(7), Cu1···Cu1′ 2.732(2), Ir···Ag 3.625 (aver.), Ir–Cu1 3.154(1), Ir–Cu1′ 3.529(1).

between both HOMOs (−6.82 eV **2**, −6.72 eV **3**) is in line with the experimental trend. Thus, the easier oxidation of **3** can be understood by the remarkable contribution of the donor C≡CR groups, which increases the energy of the HOMO. In both derivatives, the lowest-energy unoccupied orbitals (LUMO to LUMO+3) are mainly located on the π* orbitals of the ppy units (92–94% **2**, 96% **3**), the main difference being that in **2** the ppy units contributing to each orbital are associated to the same Ir^{III} complex, while in **3** they are distributed over all the four ppy ligands.

The photophysical properties of **2** and **3** were investigated and compared to that of **1**. Representative emission spectra are shown in Fig. 2. The UV-vis absorption spectra of **2** and **3** are similar and closely comparable to that of the precursor **1** (Fig. S22†) with only slight blue shifts in the low energy region [395 nm (**2**), 392 nm (**3**), and 406 nm (**1**)]. Previous studies on $[Ir_2(ppy)_4(\mu\text{-}C{\equiv}CTol)_2]$[5] and TD-DFT analyses now conducted on optimized structures of **2** and **3** were used to interpret these spectra (Table S10, Fig. S27†). In particular, the high-energy absorptions (λ<290 nm) are ascribed to typical π–π* ligand centred transitions at the ppy and alkynyl moieties. The calculated transitions by TD-DFT agree reasonably well with the experimental data, although the low energy bands at 395 (**2**) and 392 nm (**3**) are not properly computed. The lowest energy band of **2** are composed of four transitions (314–325 nm) from HOMO, HOMO−1, and HOMO−6, which are mainly contributed by the Ir^{III} and ppy units (40–84% ppy, 5–41% Ir^{III} and 12–17% alkynyl fragment), to the LUMO to LUMO+3, which are mainly distributed on the ppy units. Therefore, this band is assigned as a mixture of ^{1}ILCT and ^{1}MLCT with some ^{1}L′LCT (alkynyl to ppy) character. The first singlet–singlet transition in **3** is slightly blue shifted and computed at 321 nm, in line with the experimental values. The lowest energy band is composed of four transitions (315–321 nm) from HOMO (Ir^{III} 34%; ppy 22%; C≡CR 36%; Cu^I 8%) and HOMO−1 (Ir^{III} 40%; ppy 28%; C≡CR 24%; Cu^I 8%) to LUMO to LUMO+3, which are distributed over all the four π* orbitals (ppy 96%). This band is attributed to Ir^{III}/Cu^I/C≡CR/ppy → ppy transitions, having a mixed ^{1}MLCT and ^{1}L′LCT character.

Both clusters are moderate phosphorescent emitters in rigid and fluid media with lifetimes in the microsecond regime, whereas **1** is only weekly emissive in fluid and glassy solution – Table S6.† In detail, **1** shows a slightly structured band – *ca.* 525 nm – both at 298 and 77 K (Fig. S23†), which is ascribed to a mixture of ^{3}MLCT/^{3}L′LCT (L = ppy; L′ = C≡CR) according to the previous theoretical calculations.[5] Similarly, **2** emits in the green region at 298 K (480–515 nm, Fig. 2 and S24†). In glassy solution, the emission becomes well-structured and is significantly blue shifted in relation to **1** (475 **2** *vs.* 520 nm **1**), indicating that the emission in the cluster has a more ^{3}LC character.

The photoluminescence quantum yield of **2** in solution is triple that of **1** (ϕ = 1.8 **2** *vs.* 0.6% **1**) and is remarkably enhanced in the solid state (ϕ = 7%). Doped in a poly(methyl methacrylate) (PMMA) film, **2** displays similar green emission (Fig. 2), with increase in ϕ = 23% at low concentration (10 wt%). Upon increasing the complex concentration, the peak maxima shifts slightly to the red and the ϕ progressively decreases (Fig. S26†), due to the well-known self-quenching process.[5]

In stark contrast to **2**, the emission of **3** is placed in the orange region (620–600 nm, Fig. 2 and S25†). The remarkable red shift and unstructured shape of the band is unequivocally a result of the involvement of the Cu-π-alkynyl in the emitting excited state. The ϕ value is similar to that of **2** in solution (ϕ = 1.8%), but is notably greater in the solid state (ϕ = 18%). In doped PMMA films, the influence of the concentration is opposite to that observed in **1**, enhancing with increasing doping concentration (Fig. S26†), pointing to a different emissive state.

To get a further understanding of the distinctive emission properties of both clusters, the geometries of the lowest T_1 states were optimized in the gas phase (Tables S7 and S8†). Negligible structural changes were observed in the computed T_1 state for **2** in relation to the ground state (S_0) geometry, which is in agreement with the small Stokes shift found in the emission. The SOMO and SOMO−1 are primarily located on one of the phenylpyridinate groups with a small contribution of the Ir^{III} and the alkynyl ligands (Fig. 3 and Table S11†) and,

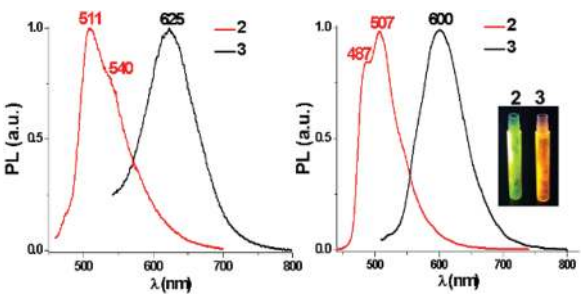

Fig. 2 Normalized emission spectra of **2** and **3** in THF (10^{-4} M) (left) and in PMMA (10%) (right) at 298 K.

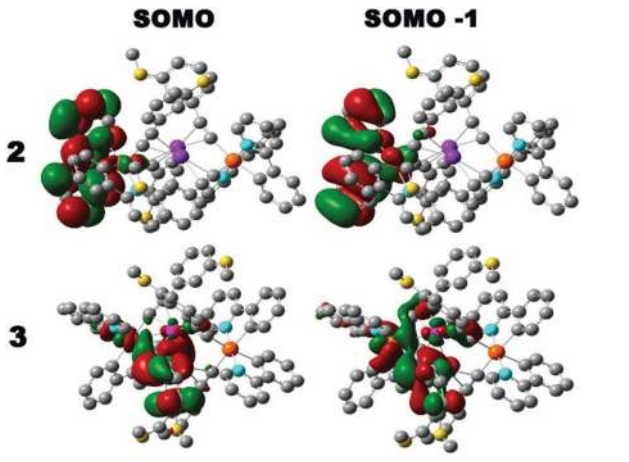

Fig. 3 Molecular orbital topology for the computed T_1 states of **2** and **3**.

consequently, the emissive state of this cluster has mainly a ^{3}LC nature with a minor ^{3}MLCT character. The calculated emission energy is estimated at 495 nm, in agreement with the values obtained in the solid-state (515 nm) and PMMA (487 and 507 nm). To our surprise, a remarkable structural distortion was found in the T_1 of **3** compared to that of S_0. As shown in Fig. S30,† upon photoexcitation, the ligation of one of the C≡C–R units change from μ–$\eta^1(Ir^{III})$:$\eta^2(Cu^I)$ to μ_3–$\eta^1,\eta^1,\eta^1(Ir^{III},Cu^I,Cu^I)$, which is also reflected in the notable bend at the C_α atom (Ir1′C10′C11′ 143.11° in T_1 *vs.*: 162.14° in S_0). As a consequence, the $Cu^I\cdots Cu^I$ separation (Δ 0.172 Å) and the $Cu^I\cdots Ir^{III}$ distances to one of the "$Ir(C{\equiv}CC_6H_4OMe\text{-}3)_2$" fragments decrease considerably ($Ir^{III}\cdots Cu^{I\prime}$ 2.725 Å in T_1 *vs.* $Ir^{III}\cdots Cu^{I\prime}$ 2.928 in S_0). For **3**, the SOMO is primarily confined to the alkynyl group (Fig. 3), which bridges the three metals ($IrCu_2$) and bears the contribution of both Cu^I atoms having Cu^I–Cu^I bonding (C≡CR/Ir^{III}/Cu^I 73/4/13%) character. The SOMO−1 is extended over both alkynyls through the Ir^{III}(d) and has a higher metallic contribution (C≡CR/Ir^{III}/Cu^I 53/24/13%). Therefore, the emission has a ^{3}L′C alkynyl nature and an alkynyl to metal charge transfer character (^{3}L′MCT) with a higher contribution of the metal centres (^{3}MMCT) than in **2**. The computed value at 625 nm is almost identical to the one obtained experimentally in the solid-state (615 nm).

Finally, the electroluminescence features of **2** and **3** were investigated in single-layer lighting devices. Owing to the simple device preparation and optimization compared to OLEDs, we decided to follow a recent approach based on the design of host–guest LECs (see the ESI† for more details and references) with an active layer that consists of an electroactive host matrix doped with mobile anions in the form of ionic liquids with the emitter. As shown in Fig. 4, the electroluminescence features of both clusters are similar to those noted in the photoluminescence studies, suggesting that the same T_1 state is involved under both photo- and electro-excitation conditions. In detail, devices with **2** are green emitting with the maximum at 518 nm with *x*/*y* colour coordinates of 0.29/044, while devices with **3** shows a broad orange emission centred at 625 nm and *x*/*y* colour coordinates of 0.47/0.46. Importantly, the emission of the matrix is not observed at the high-energy region (390–450 nm), suggesting an efficient energy transfer process from the matrix to the emitters. Regarding the device performance, although the brightness is moderately low, the efficiency of approximately 0.5 cd A^{-1} and the stability of several hours are encouraging with respect to the future design of this novel family of emitters in concert with the device optimization.

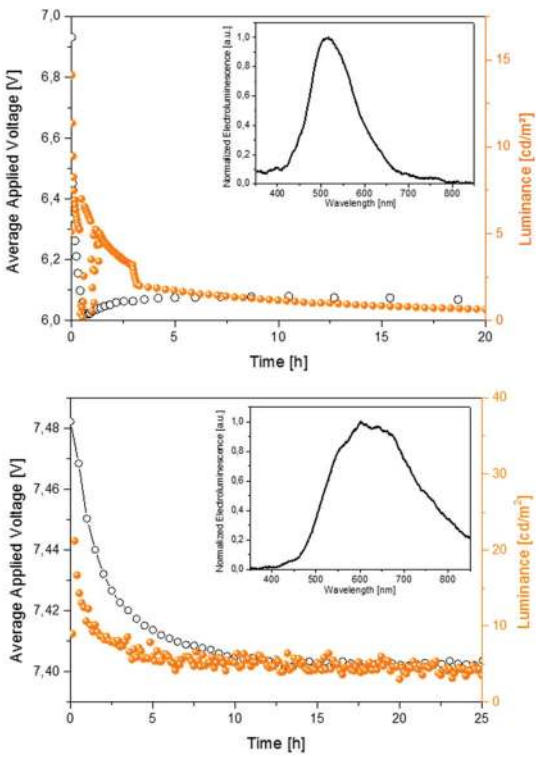

Fig. 4 Luminance and applied voltage *vs.* time of devices **2** (top) and **3** (bottom) driven with a pulsed-current of 2.5 mA. Inset graphs show the EL spectrum of the devices.

In summary, two luminescent Ir_2M_2 (M = Ag, Cu) clusters featuring iridium-bis(cyclometalated) fragments and $C{\equiv}CC_6H_4OMe$-3 connecting the metal centers are reported for the first time. In addition, their distinct photo- and electroluminescence behavior provides an interesting example of the role of the alkynyl groups in modulating metallophillic bonding in the excited state. This new family of clusters provides new opportunities to achieve color tuning with potential in the field of optoelectronics and further work is currently in progress to study the formation, structures and properties of other Ir–M clusters, as well as the device optimization.

This work was supported by the Spanish MINECO/FEDER (CTQ2013-45518-P). R. D. C. and M. D. W. acknowledge funding from DFG Excellence 'Engineering of Advanced Materials' (EAM) and the Fonds der Chemischen Industrie (FCI) in the Liebig grant framework. P. M. and N. G. thank to the UR for a grant. We thank CESGA for computer support.

Notes and references

1 (*a*) Y. You and W. Nam, *Chem. Soc. Rev.*, 2012, **41**, 7061; (*b*) C. L. Ho and W. Y. Wong, *New J. Chem.*, 2013, **37**, 1665; (*c*) S. Ladouceur and E. Zysman-Colman, *Eur. J. Inorg. Chem.*, 2013, **17**, 2985; (*d*) L. Xiao, Z. Chen, B. Qu, J. Luo, S. Kong, Q. Gong and J. Kido, *Adv. Mater.*, 2011, **23**, 926; (*e*) R. D. Costa, E. Ortí, H. J. Bolink, F. Monti, G. Accorsi and N. Armaroli, *Angew. Chem., Int. Ed.*, 2012, **51**, 8178; (*f*) S. B. Meier, D. Tordera, A. Pertegás, C. Roldán-Carmona, E. Ortí and H. J. Bolink, *Mater. Today*, 2014, **17**, 217; (*g*) Z. Yu, L. Li, H. Gao and Q. Pei, *Sci. China: Chem.*, 2013, **56**, 1075.

2 (*a*) Y. Chi and P. T. Chou, *Chem. Soc. Rev.*, 2010, **39**, 638; (*b*) J. A. G. Williams, A. J. Wilkinson and V. L. Whittle, *Dalton Trans.*, 2008, 2081.

3 (*a*) R. Muñoz-Rodríguez, E. Buñuel, N. Fuentes, J. A. G. Williams and D. J. Cárdenas, *Dalton Trans.*, 2015, **44**, 8394; (*b*) V. H. Nguyen, R. S. H. Khoo and J. H. K. Yip, *Inorg. Chem.*, 2015, **54**, 2264; (*c*) Y. Zheng, A. S. Batsanov, M. A. Fox, H. A. Al-Attar, K. Abdullah, V. Jankus, M. R. Bryce and A. P. Monkman, *Angew. Chem., Int. Ed.*, 2014, **53**, 11616; (*d*) L. Donato, C. E. McCusker, F. N. Castellano and E. Zysman-Colman, *Inorg. Chem.*, 2013, **52**, 8495; (*e*) E. Baranoff, E. Orselli, L. Allouche, D. Di Censo, R. Scopelliti, M. Grätzel and M. K. Nazeeruddin, *Chem. Commun.*, 2011, **47**, 2799.

4 (*a*) V. W.-W. Yam, V. K.-M. Au and S. Y.-L. Leung, *Chem. Rev.*, 2015, **115**, 7589; (*b*) W. Wang and H.-B. Yang, *Chem. Commun.*, 2014, **50**, 5171; (*c*) H. Lang, A. Jakob and B. Milde, *Organometallics*, 2012, **31**, 7661; (*d*) V. W.-W. Yam and K. M.-C. Wong, *Chem. Commun.*, 2011, **47**, 11579; (*e*) J. C. Lima and L. Rodríguez, *Chem. Soc. Rev.*, 2011, **40**, 5442; (*f*) J. R. Berenguer, E. Lalinde and M. T. Moreno, *Coord. Chem. Rev.*, 2010, **254**, 832; (*g*) I. S. Krytchankou, I. O. Koshevoy, V. V. Gurzhiy, V. A. Pomogaev and S. P. Tunik, *Inorg. Chem.*, 2015, **54**, 8288; (*h*) J. R. Berenguer, J. Fernández, B. Gil, E. Lalinde and S. Sánchez, *Chem. – Eur. J.*, 2014, **20**, 2574; (*i*) W.-J. Guo, Y.-T. Wang, D.-X. Kong, J.-Y. Wang, Q.-H. Wei and G.-N. Chen, *Chem. – Eur. J.*, 2015, **21**, 4205; (*j*) Y. Wang, H. Su, C. Xu, G. Li, L. Gell, S. Lin, Z. Tang, H. Häkkinen and N. Zheng, *J. Am. Chem. Soc.*, 2015, **137**, 4324.

5 J. Fernández-Cestau, N. Giménez, E. Lalinde, P. Montaño, M. T. Moreno and S. Sánchez, *Organometallics*, 2015, **34**, 1766.

6 (*a*) M. I. Bruce, N. N. Zaitseva, B. W. Skelton, N. Somers and A. H. White, *Aust. J. Chem.*, 2003, **56**, 509; (*b*) I. Ara, J. R. Berenguer, E. Eguizábal, J. Forniés, E. Lalinde and A. Martín, *Eur. J. Inorg. Chem.*, 2001, 1631; (*c*) J. R. Shakirova, E. V. Grachova, A. S. Melnikov, V. V. Gurzhiy, S. P. Tunik, M. Haukka, T. A. Pakkanen and I. O. Koshevoy, *Organometallics*, 2013, **32**, 4061; (*d*) Y. Jiang, W.-J. Guo, D.-X. Kong, Y.-T. Wang, J.-Y. Wang and Q.-H. Wei, *Dalton Trans.*, 2015, **44**, 3941; (*e*) I. Meana, P. Espinet and A. C. Albéniz, *Organometallics*, 2014, **33**, 1.

7 (*a*) P. Pyykkö, *Chem. Rev.*, 1997, **97**, 597; (*b*) H. Schmidbaur and A. Schier, *Angew. Chem., Int. Ed.*, 2015, **54**, 746; (*c*) S. Sculfort and P. Braunstein, *Chem. Soc. Rev.*, 2011, **40**, 2741.